ROUGH TURBULENT BOUNDARY LAYER IN WAVE-CURRENT COMBINED MOTION

Supharatid*, S., Tanaka**, H., and Shuto***, N.

Experimental and numerical investigations are carried out for waves with following and opposing currents. The flume bottom is covered by triangular strip roughnesses. The K-ε model is solved, for the large Reynolds number flow, with the Galerkin finite element method. Profiles and time series of the ensemble-averaged horizontal velocity are well predicted except in the very vicinity of the bottom. Magnitude but phase of the r.m.s. velocity fluctuations is reasonable predicted. Time-mean horizontal velocity and r.m.s. horizontal velocity fluctuation are also well predicted. The measured data give a much smaller von Karman constant which is not predicted by the model.

Keyword : turbulent boundary layer, wave-current, K-ε model

I INTRODUCTION

Turbulent transport in the combined flow of surface gravity waves and currents plays a dominant role in many physical processes: e.g. sediment erosion and deposition. The boundary layer flow for current in the presence of wave is also of special interest since a current with waves represents the most essential hydrodynamic flow condition with respect to sediment transport.

Knowledge on the oscillatory boundary layer has been accumulated by many researchers. A recent review can be found in Sleath[7]. There are many numerical models: e.g. Sheng[5] and Davies et al.[1]. Sawamoto and Sato[8] carried out the same kind of experiment as Sleath[6]. Their works were concentrated on the detailed structure of turbulence and the applicability of turbulence models.

Experimental study of turbulence in the wave-current combined motion are few. In the work of Kemp and Simons[2,3], the velocities and turbulence quantities were measured with an LDA. However, the detail of the effects of waves on the current is not given. So far, a comparison of numerical study with the experiments, especially in terms of the turbulence quantities, have not been made.

In order to understand the flow and the turbulent characteristics under the interaction between waves and current, experimental and numerical investigations are carried out in the present paper. Unlike the works of Kemp and Simons, the present study treats rather large wave height. Results from the experiments are compared with the detailed numerical results by the K-ε model developed by the authers.

II EXPERIMENT AND THEORY

2.1 Experiment

The experiments are carried out in a wave tank (see Fig. 1): 14.5 m long, 30 cm wide, and 55 cm deep. A piston-type wave generator is used to generate surface gravity waves. The flume bottom is covered with triangular strip roughness. The detail of the experimental

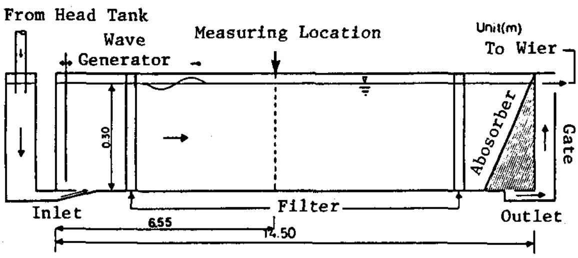

Fig. 1 Experimental set-up

* M.Eng, Graduate student, Dept. of Civil Eng., Tohoku Univ.
** Dr. Eng, Assoc. Prof., Asian Inst. of Tech.
*** Dr. Eng, Prof., Disaster Control Research Center, Tohoku Univ.

set-up can be found in Supharatid et al.[9]. The particle velocities are measured at one location (up to 18 points in the vertical) between roughness spacings by an LDV. The measurements cover the data of 50 wave periods. The water depth is kept constant at 30 cm, throughout the study. The experimental conditions are given in Table 1.

2.2 Theory

By assuming that the boundary layer thickness is much smaller than the wave length ($k\delta_w \leq 1$) and neglecting terms of the order of $O(ka_m)$, a set of equations can be expressed in the Cartesian co-ordinates (see Fig. 2) as follows:

$$\frac{\partial V}{\partial t} = \frac{\partial}{\partial z}\{\nu_e \frac{\partial V}{\partial z}\} + S_U \qquad (1)$$

where k = wave number
a_m = excursion amplitude
V = transport variables
ν_e = effective eddy viscosity
S_U = source or sink term

Table 1 Experimental Conditions

Flow dir.	U_c (cm/s)	T (sec)	D (cm)	H (cm)	z_0 (mm)	RE ($U_0 a_m/\nu$)
Fol.	11.93	1.3	30	9.41	0.54	10014
Opp.	14.74	1.3	30	9.75	0.61	7569

Equation (1) is used on employing the eddy viscosity concept that the Reynolds stress is related to the mean rate of strain through the turbulent viscosity, ν_t,

$$\overline{-u'w'} = \nu_t \frac{\partial u}{\partial z}, \quad \overline{-v'w'} = \nu_t \frac{\partial v}{\partial z} \qquad (2)$$

Terms V, ν_e, and S_U in the governing equations represent the following quantities.

In the momentum equation in the x- and y-directions, they are:

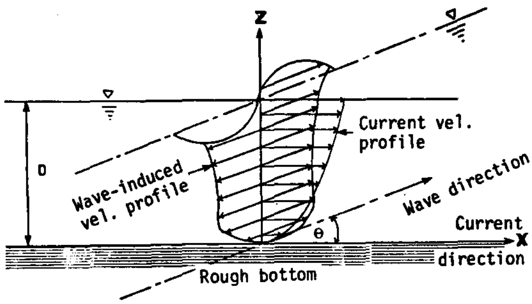

Fig. 2 Definition sketch

$$V = u, S_U = -\frac{1}{\rho}\frac{\partial p_w}{\partial x} - \frac{1}{\rho}\frac{\partial p_c}{\partial x}, \nu_e = \nu + \nu_t \qquad (3)$$

$$V = v, S_U = -\frac{1}{\rho}\frac{\partial p_w}{\partial y}, \nu_e = \nu + \nu_t \qquad (4)$$

Table 2 Model constants

C_μ	$C_{1\varepsilon}$	$C_{2\varepsilon}$	σ_k	σ_ε
0.09	1.44	1.92	1.0	1.3

where u and v are the velocities in the x- and y-directions. p_w and p_c are the water pressure for the waves and a steady current respectively.

The pressure gradient for waves and a steady current are expressed as:

$$-\frac{1}{\rho}\frac{\partial p_w}{\partial x} = \frac{\partial U_\alpha}{\partial t}, \quad -\frac{1}{\rho}\frac{\partial p_w}{\partial y} = \frac{\partial V_\alpha}{\partial t} \qquad (5)$$

$$-\frac{1}{\rho}\frac{\partial p_c}{\partial x} = \frac{u^2_{*c}}{D} \qquad (6)$$

where $(U_\alpha, V_\alpha) = U_w(\cos\theta, \sin\theta)$, U_w is the free stream velocity of the wave-induced motion. u_{*c} is the bottom friction velocity (for a steady current) estimated from a logarithmic velocity distribution(Eq. (7)). D is the mean water depth.

$$u_{*c} = \kappa U_c / \ln(D/ez_0) \qquad (7)$$

Table 3 Dimensionless variables

Dimensional variables	Dimensionless variables
u	$u/\dot{U}_w$
v	$v/\dot{U}_w$
K	$K/\dot{U}_w^2$
ε	$\varepsilon/\omega\dot{U}_w^2$
$-u'w'$	$-u'w'/\dot{U}_w^2$
t	ωt
ν	$\nu\omega/\dot{U}_w^2$
ν_t	$\nu_t\omega/\dot{U}_w^2$
L_d	$L_d\omega/\dot{U}_w$
z	z/D

where U_c = depth-average steady current velocity
z_0 = bottom roughness height, κ = von Karman constant
e = 2.718 (Base of the natural logarithm)

For the turbulent energy K, variables are:

$$V = K, \quad S_U = \nu_t\{(\frac{\partial u}{\partial z})^2 + (\frac{\partial v}{\partial z})^2\} - \varepsilon, \quad \nu_e = \nu + \frac{\nu_t}{\sigma_k} \tag{8}$$

For the turbulent energy dissipation rate ε, variables are:

$$V = \varepsilon, \quad S_U = C_{1\varepsilon}\frac{\varepsilon}{K}\nu_t\{(\frac{\partial u}{\partial z})^2+(\frac{\partial v}{\partial z})^2\} - C_{2\varepsilon}\frac{\varepsilon^2}{K}, \quad \nu_e = \nu_t + \frac{\nu_t}{\sigma_\varepsilon} \tag{9}$$

The closure scheme is completed by the turbulence scaling law,

$$\nu_t = C_\mu K^2/\varepsilon \tag{10}$$

where $C_{1\varepsilon}$, $C_{2\varepsilon}$, σ_k, σ_ε, and C_μ are model constants given in Table 2.

III SOLUTION METHOD

The above equations are solved with the Galerkin finite element method. The element residuals , R_U, for Eq. (1) can be expressed as:

$$R_U = \int_{\Omega_e}\frac{\partial V}{\partial t}N_i\,d\Omega_e + \int_{\Omega_e}\nu_e\frac{\partial V}{\partial z}\frac{\partial N_i}{\partial z}d\Omega_e - \int_{\Gamma_e}\nu_e\frac{\partial V}{\partial z}N_i\,l_z\,d\Gamma_e - \int_{\Omega_e}S_U N_i\,d\Omega_e \tag{11}$$

Here Ω_e is the element domain. Γ_e is the element boundary. A linear Galerkin weighting function, N_i, is selected for the present one-dimentional problem. l_z is the direction cosines. For simplicity, all variables are nondimensionalized by the amplitude of the free stream velocity of the wave-induced motion ($\hat{U}_\omega$), the fundamental wave frequency (ω), and the mean water depth (D) as given in Table 3.

In order to increase the accuracy of the computation near the bottom, the vertical spatial grid is made equi-spaced in a logarithmic scale. The following relation transforms the actual height z to ζ for the computation.

$$\zeta = \frac{\ln z/z_0}{\ln D/z_0} \tag{12}$$

The initial condition for u is the conventional log-profile. For K and ε, the empirical expressions for steady uniform current suggested by Nezu and Nakagawa[4] are used. They are:

$$u(z,0)/u_{*c} = (1/\kappa)\ln(z/z_0) \tag{13}$$

$$K(z,0)/u_{*c} = 4.78\exp(-2z/D) \tag{14}$$

$$\varepsilon(z,0)D/u_{*c} = 9.76\exp(-3z/D)/(z/D)^{1/2} \tag{15}$$

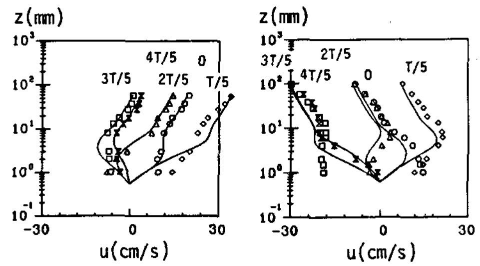

Fig. 3 Profile of the ensemble-averaged horizontal velocity

The boundary conditions are as follows:

At the lower boundary,

$$u = 0, \quad v = 0,$$

$$\partial K/\partial z = 0,$$

$$\varepsilon = C_\mu^{3/2}K^{3/2}/L_d \tag{16}$$

where $L_d = \kappa z_0$

At the upper boundary,

$$u = U_{c\alpha} + U_\alpha, \quad v = V_\alpha,$$

$$\partial K/\partial z = 0, \quad \partial\varepsilon/\partial z = 0 \tag{17}$$

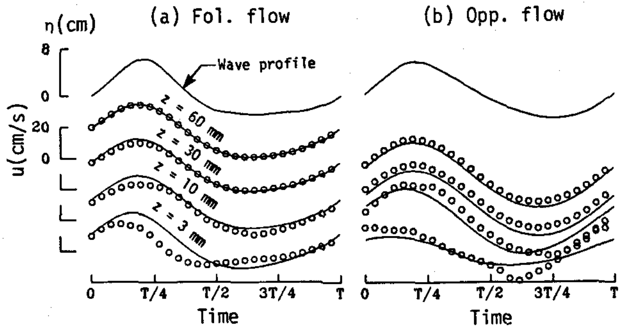

Fig. 4 Time histories of the ensemble-averaged horizontal velocity

where $U_{c\infty}$ is a steady current velocity at the upper boundary. The lower boundary is located at the roughness height. The upper boundary conditions are applied at an elevation where there is a significant reduction in the time-mean turbulent intensities.

IV RESULTS

The following comparisons are only for the co-directional waves and currents.

(4.1) Ensemble-averaged horizontal velocity profile.

Figures 3(a) and 3(b) show profile of the ensemble-averaged horizontal particle velocity for waves with following and opposing currents. Agreements with the measured data are generally good. However, the discrepancies are found in the vicinity of the bottom ($z \leq 2$ mm). These near-bottom velocities are not predicted well, because the characteristic roughness height is obtained from the steady current alone and is assumed to be constant during the whole wave cycle. In addition, the present model does not account for the moderate and low Reynolds number effect.

(4.2) Time histories of the ensemble-averaged horizontal velocity

The corresponding time histories of the ensemble-averaged horizontal velocity are presented in Figs. 4(a) and 4(b). Good agreements are found at $z \geq 10$ mm. In the vicinity of the bottom, the predicted values are found deviated from the measured data, especially near the phases of the passage of wave crest and wave trough. However, the model simulates relatively well the phase advance of the near-bottom velocity.

(4.3) Time histories of r.m.s. velocity fluctuations

The calculations yield the variation of K in time and space, but not each of the velocity fluctuations. Therefore, the predicted values of K are distributed into three components on using the relationship obtained by Townsend[10], i.e. $u'^2 : v'^2 : w'^2 = 0.45 : 0.21 : 0.34$.

Time histories of the r.m.s. value of velocity fluctuation at different levels are presented in Figs. 5 and 6. Both the predicted $\sqrt{u'^2}$ and $\sqrt{w'^2}$ fluctuate periodically in the boundary layer, and become less phase dependent far away from the bottom. Above the elevation of 5 mm, the values of $\sqrt{u'^2}$ and $\sqrt{w'^2}$ remain almost constant over the wave cycle. The magnitude of $\sqrt{w'}$ is somewhat overpredicted.

One important feature is a pronounced asymmetry of the predicted velocity fluctations in the wave cycle. For the follow-

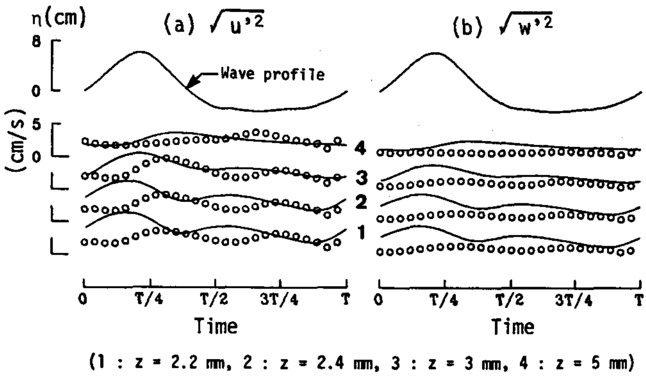

Fig. 5 Time histories of r.m.s. velocity fluctuations (Fol. flow)

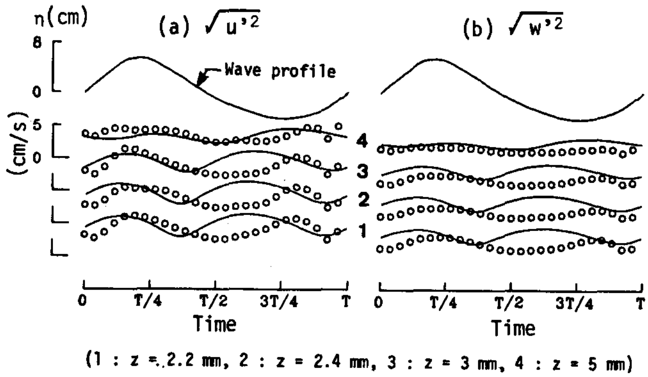

Fig. 6 Time histories of r.m.s. velocity fluctuations (Opp. flow)

ing (opposing) flow, the greater magnitude is found under the wave crest (trough) than under the wave trough (crest). The maximum value of $\sqrt{u'^2}$ or $\sqrt{w'^2}$ occurs at different phases at different heights. The phase variations are not predicted well. The measured data near the bottom are behind or in phase with the surface profile, while the predicted results always show a phase advance.

(4.4) Time-mean horizontal velocity.

Results of time-mean velocity profiles are presented in Fig. 7. Comparisons of the measured data between the steady current and the time-mean wave-current show that there are some significant departures. The reductions near the bottom are found, i.e. within about two ripple heights (≃ 10 mm) for the following flow and upto 10 ripple heights (≃ 40 mm) for the opposing flow. When waves are superposed on a current, the mean flow is retarded as a result of the additional effects of the bottom friction.

The model predicts well for the case of the following flow. For the case of the opposing flow, agreements are not so good, in particular, below the level of flow reversal (z < 5 mm). In both cases, the model reproduces very well two parts of the logarithmic profiles, i.e upper and lower parts. The reversion in the direction of current is observed for the opposing flow. This might be generated under strong effects of vortex formations and ejections from the roughness crest during the wave cycle.

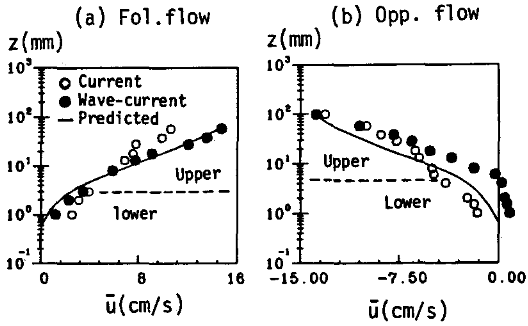

Fig. 7 Time-mean horizontal velocity

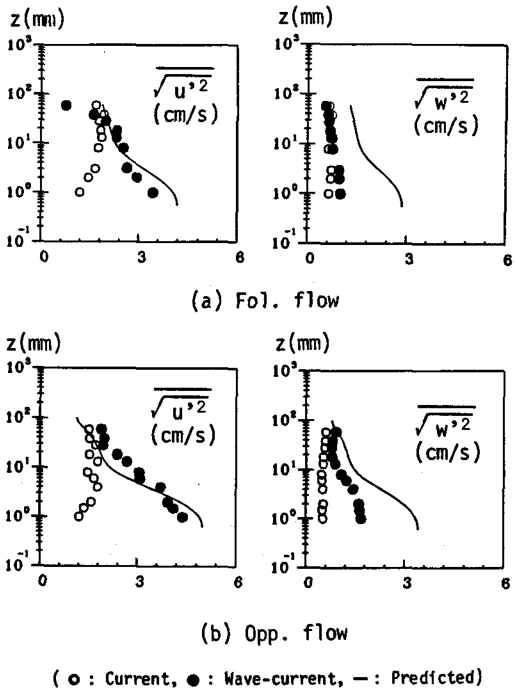

Fig. 8 Time-mean r.m.s. velocity fluctuations

(4.5) Time-mean r.m.s. velocity fluctuations

Figure 8 presents the time-mean value of the r.m.s. velocity fluctuations. The measured data reveal that the effect of waves causes significant increases in $\sqrt{u'^2}$ and $\sqrt{w'^2}$ near the bottom. The turbulence level becomes low above a depth of 30 mm, even lower than that for the steady current in the case of following flow. In the case of the opposing flow, Both $\sqrt{u'^2}$ and $\sqrt{w'^2}$ do not show any reduction but increases throughout the depth by the addition of waves to the current.

The model, generally, shows good predictions of $\sqrt{u'^2}$. There are deviations in the profiles of $\sqrt{w'^2}$.

(4.6) Time-mean eddy viscosity

An interesting and useful quantity is the eddy viscosity. Its time-mean value (opposing flow), $\overline{\nu_t} = -\overline{u'w'}/\partial\bar{u}/\partial z$ is presented in Fig. 9. Also included is values for the steady current. The measured data displays an increase from the bottom. There is indeed a linear profile near the bottom for which $\bar{\nu}_t \propto u_{*s}z$ where u_{*s} is the mean bottom friction velocity.

Line 1 is obtained with the K-ε model. Lines 2 and 3 are for, $\bar{\nu}_t = \kappa u_{*s} z$, where u_{*s} is obtained from the measured Reynolds stress and the log-fitting to the time-mean velocity profile, respectively. Line 1 shows a slight suppression near the wave boundary layer (≃ 10 mm).

The theoretical profiles do not match well with the experiments. The measured data in the present study gives the von Karman constant, κ, ranging from 1/5 to 1/10 of the usual value, which is the same as in case of an oscillatory flow by Sleath (1987).

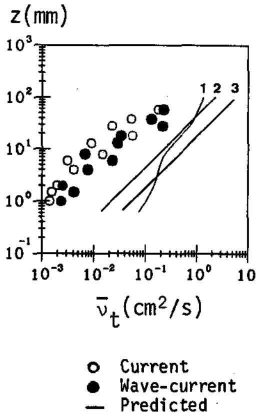

Fig. 9 Time-mean eddy viscosity

V CONCLUSIONS

Experimental investigations on the wave-current interaction within the rough bottom layer are carried out. The K-ε model is used to simulate this phenomenon by the application of the finite element method.

Generally good agreements are obtained, especially, in the time-mean flow properties such as the time-mean velocity and turbulent intensities. The distinct differences in the velocity and turbulent intensities, during the phases of acceleration and deceleration, are favorably predicted.

Deviations of the predicted values from the measured data are found in the vicinity of the bottom where the flow always experiences a smooth bottom near the phase of the flow reversal. In order to obtain more precise results, the time-variation of the roughness height and the effects of moderate and low Reynolds number sholud be taken into consideration at this phase. In other words, the bottom boundary conditions for the turbulent kinetic energy and energy dissipation rate should be modified to account for this condition.

REFFERENCES

1) Davies, A.G. Soulsby, R.L., and King, L.H (1988): A numerical model of the combined wave and current bottom boundary layer, J, Geophys. Res., Vol. 93(C1), pp. 491-508.
2) Kemp, P.H. and Simons, R.R. (1982) : The interaction between waves and a turbulent current : wave propagating with the current, J. Fluid Mech., Vol. 116, pp. 227-250.
3) Kemp, P.H. and Simons, R.R. (1983) : The interaction of waves and a turbulent current : wave propagating against the current, J. Fluid Mech., Vol. 130, pp. 73-89.
4) Nezu, I. and Nakagawa, H. (1987) : Numerical calculation of turbulent open-channel flows in consideration of free-surface effect, Mem. Fac. Eng., Kyoto Univ., Vol. 49(2), pp. 111-145.
5) Sheng, P.T. (1984) : A turbulent transport model of coastal processes, Proc. 19th ICCE, pp. 2380-2396.
6) Sleath, J.F.A. (1987) : Turbulent oscillatory flow over rough beds, J. Fluid Mech., Vol. 182, pp. 369-409.
7) Sleath, J.F.A. (1990) : Seabed boundary layer, The Sea, Vol. 9, Ocean Engineering Science, Part B, pp. 693-727.
8) Sawamoto, M. and Sato, E. (1991) : The structure of oscillatory turbulent boundary layer over rough bed, Coast. Eng. Japan, Vol. 34., No. 1, pp. 1-14.
9) Supharatid, S., Tanaka, H., and Shuto, N. (1991) : A study on the velocity distribution under wave-current combined motion, Proc. 38th Japanese Conf. Coast. Eng., JSCE, pp. 6-10 (in Japanese).
10) Townsend, A.A. (1976) : The structure of turbulent shear flow, Cambridge Univ. Press., 429 pages.